Osteal macrophages support physiologic skeletal remodeling and anabolic actions of parathyroid hormone in bone

Sun Wook Cho[a,b], Fabiana N. Soki[a], Amy J. Koh[a], Matthew R. Eber[a], Payam Entezami[a], Serk In Park[a], Nico van Rooijen[c], and Laurie K. McCauley[a,d,1]

[a]Department of Periodontics and Oral Medicine, University of Michigan School of Dentistry, Ann Arbor, MI 48109; [b]Department of Internal Medicine, National Medical Center, Jung-gu, Seoul 100-799, Korea; [c]Department of Molecular Cell Biology, Vrije University Medical Center, 1081 HZ, Amsterdam, The Netherlands; and [d]Department of Pathology, University of Michigan Medical School, Ann Arbor, MI 48109

Edited by John T. Potts, Massachusetts General Hospital, Charlestown, MA, and approved December 10, 2013 (received for review August 21, 2013)

Cellular subpopulations in the bone marrow play distinct and unexplored functions in skeletal homeostasis. This study delineated a unique role of osteal macrophages in bone and parathyroid hormone (PTH)-dependent bone anabolism using murine models of targeted myeloid-lineage cell ablation. Depletion of c-fms$^+$ myeloid lineage cells [via administration of AP20187 in the macrophage Fas-induced apoptosis (MAFIA) mouse model] reduced cortical and trabecular bone mass and attenuated PTH-induced trabecular bone anabolism, supporting the positive function of macrophages in bone homeostasis. Interestingly, using a clodronate liposome model with targeted depletion of mature phagocytic macrophages an opposite effect was found with increased trabecular bone mass and increased PTH-induced anabolism. Apoptotic cells were more numerous in MAFIA versus clodronate-treated mice and flow cytometric analyses of myeloid lineage cells in the bone marrow showed that MAFIA mice had reduced CD68$^+$ cells, whereas clodronate liposome-treated mice had increased CD68$^+$ and CD163$^+$ cells. Clodronate liposomes increased efferocytosis (clearance of apoptotic cells) and gene expression associated with alternatively activated M2 macrophages as well as expression of genes associated with bone formation including *Wnt3a*, *Wnt10b*, and *Tgfb1*. Taken together, depletion of early lineage macrophages resulted in osteopenia with blunted effects of PTH anabolic actions, whereas depletion of differentiated macrophages promoted apoptotic cell clearance and transformed the bone marrow to an osteogenic environment with enhanced PTH anabolism. These data highlight a unique function for osteal macrophages in skeletal homeostasis.

The skeleton provides not only physical support but also housing for numerous subtypes of hematopoietic and immune cells. Several lines of evidence suggest that these skeletal and hematopoietic systems in the bone microenvironment are not only structurally adjacent, but also functionally interactive (1–4). Maintenance of the hematopoietic stem cell niche and B-lymphocyte differentiation has been attributed to osteoblasts (1, 2, 5). T lymphocytes support anabolic actions of parathyroid hormone (PTH) in bone via production of osteoblast stimulating Wnt-10b (6).

Daily intermittent parathyroid hormone (PTH 1–34) administration has prominent anabolic actions in bone and is currently the only approved anabolic agent in the United States for the treatment of osteoporosis. PTH also supports the hematopoietic system by stimulating osteoblastic production of several cytokines, including IL-6 (7, 8), CXCL12 (9), MCP-1 (also known as CCL2) (10, 11), and the soluble IL-6 receptor (sIL6R) (4). PTH improved the success rate of hematopoietic stem cell (HSC) engraftment in hematopoietic malignancies and autoimmune diseases via supporting HSC repopulation of the marrow (12–14). The dependence of hematopoietic lineage cells for PTH anabolic actions is unknown.

Macrophages are mononuclear cells of the myeloid lineage derived from HSCs. Different types of tissue-resident macrophages include Kupffer cells in the liver, Langerhans cells in the lung, and microglia in the brain. In bone, resorbing osteoclasts have been considered the tissue-resident macrophages. However, recent data showed that distinct from osteoclasts bone contains other resident macrophages, especially in the endosteal and periosteal areas (15). These "osteal" macrophages support osteoblast differentiation and mineralization in vitro (15) and play a role in intramembranous bone healing at fracture sites (16). Furthermore, osteal macrophages contribute to the maintenance of the endosteal HSC niches, and loss of osteal macrophages results in the egress of HSCs to the bloodstream (17). Collectively, osteal macrophages play novel roles in both skeletal and hematopoietic systems, yet knowledge of their functional capacities is limited. PTH anabolic actions have been linked to cells of the myeloid lineage via osteoblast derived sIL6R and Stat3 phosphorylation of CD11b$^+$ cells (4). The purpose of this study was to investigate the role of osteal macrophages in bone remodeling and anabolic actions of PTH in bone.

Results

Osteal Macrophages Were Augmented in PTH-Treated Bones. To investigate the role of osteal macrophages in anabolic actions of PTH in bone, changes in myeloid cells with PTH treatment were determined in vivo. Mice (16 wk old, female) were treated with intermittent PTH (50 μg/kg, daily s.c. injection) or saline for 4 wk and immunohistochemical F4/80 staining was performed. F4/80$^+$ osteomacrophages, characterized by spindle-shaped, elongated cytoplasm (15), formed a canopy-like structure over the cuboidal-shaped, bone-lining osteoblasts in endosteal regions of PTH-treated bones (Fig. 1*A*). In periosteal regions, PTH treatment resulted in increased cellularity of relatively cuboidal-shaped bone-lining cells and recruited F4/80$^+$osteal macrophages that

Significance

Cellular subpopulations in the bone marrow play distinct and unexplored functions in the regulation of the skeleton. A type of blood cell that resides in the bone marrow termed "osteal macrophage" was found to play a role in bone homeostasis by supporting bone formation and mediating parathyroid hormone-dependent bone regeneration. Furthermore, induction of cell death in mature macrophages activated the specialized process of efferocytosis (clearance of dead and dying cells), leading to a marrow microenvironment that supported bone formation.

Author contributions: S.W.C. and L.K.M. designed research; S.W.C., F.N.S., A.J.K., M.R.E., P.E., S.I.P., and L.K.M. performed research; N.v.R. and L.K.M. contributed new reagents/analytic tools; S.W.C., M.R.E., P.E., S.I.P., and L.K.M. analyzed data; and S.W.C., A.J.K., S.I.P., and L.K.M. wrote the paper.

The authors declare no conflict of interest.

This article is a PNAS Direct Submission.

[1]To whom correspondence should be addressed. E-mail: mccauley@umich.edu.

This article contains supporting information online at www.pnas.org/lookup/suppl/doi:10.1073/pnas.1315153111/-/DCSupplemental.

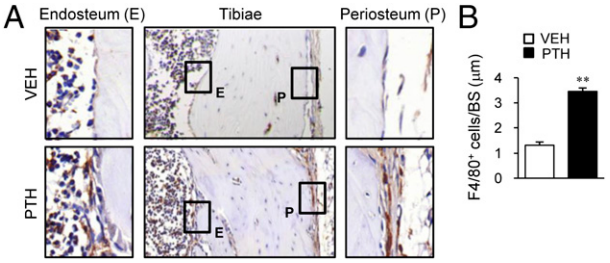

Fig. 1. Osteal macrophages in PTH actions in bone. Mice (16 wk old, female) were treated with intermittent PTH (50 μg/kg) or saline for 4 wk. Tibiae were stained for mouse F4/80. (*A*) Representative images are shown. (*Insets*) Enlarged views of F4/80$^+$ cells (brown stain) in endosteal (E) and periosteal (P) areas. (*B*) Numbers of F4/80$^+$ cells per bone surface in endosteal regions. $n = 6$ per group. $^{**}P < 0.01$ versus vehicle.

covered the periosteal lining cells. In contrast, control bones showed relatively flattened bone-lining cells with few F4/80$^+$ osteal macrophages in endosteal and periosteal areas. Numbers of F4/80$^+$ cells on endosteal bone surfaces were 2.6-fold higher in PTH versus vehicle ($P < 0.01$, Fig. 1*B*). Collectively, osteal macrophages were augmented and in close proximity to PTH-dependent bone remodeling sites, suggesting a role of osteal macrophages in anabolic actions of PTH in bone.

Depletion of Myeloid Cells in MAFIA Mice. The macrophage Fas-induced apoptosis (MAFIA) transgenic mouse model, in which the *Csf1r* (also known as *c-fms*) promoter is engineered to express a *Fas*-based inducible suicide gene and enhanced green fluorescent protein, was used for the depletion of macrophages. With AP20187 ligand injection, systemic and reversible elimination of c-fms$^+$ myeloid lineages was induced (18). After three consecutive days of initial AP20187 (10 mg/kg) injections, 16-wk-old female mice attained greater than 80% depletion of c-fms$^+$ cells as measured via flow cytometric analyses (Fig. S1).

Anabolic Actions of PTH in Macrophage-Depleted MAFIA Mice. Because anabolic effects of PTH in adult murine bone are clearly seen at 6 wk of treatment, the AP20187 ligand injection regimens were optimized for long-term depletion of c-fms$^+$ cells. As shown in Fig. 2*A*, three consecutive injections of AP20187 (10 mg/kg) were followed by booster (1 mg/kg) injections every third day for 3 wk, at which point the dose was reduced to 0.5 mg/kg for the final 3 wk. In preliminary experiments, a higher dose of AP20187 injections in young mice (8–29 d) (five consecutive injections of AP20187 followed by booster injections every other day for 3 wk) resulted in an osteopetrotic phenotype with marked suppression of serum bone turnover markers TRAP5b and P1NP (Fig. S2).

After 6 wk of depletion with the regimen in Fig. 2*A*, the MAFIA mice demonstrated grossly white bones (Fig. 2*B*) with mild anemia (24% decreased percentage of hematocrit). Immunohistochemical F4/80 staining showed a marked reduction of brown-stained macrophages in the bone marrow (Fig. 2*C*), and H&E staining demonstrated extramedullary hematopoiesis in spleen and liver (Fig. S3). Furthermore, flow cytometric analyses showed that mature macrophages displaying the specific GR1$^-$F4/80$^+$c-fms^{int}SSC$^{int/lo}$ markers (19, 20) (Fig. S4) were reduced by 85% (Fig. 2*D*) and CD68$^+$ cells, phagocytosing macrophages (21), by 48% (Fig. 2*E*). Serum bone resorption marker TRAP5b showed a 20% reduction at 2 wk, which was restored at 4 wk in the AP20187 group compared with control (Fig. 2*F*). Serum P1NP, a marker for bone formation, was suppressed 70% at 2 wk and 50% at 4 wk with AP20187 treatment (Fig. 2*G*).

Having confirmed the feasibility of long-term depletion of macrophages in the MAFIA mouse model, 6-wk intermittent PTH (50 μg/kg, daily s.c. injection) was administered after the initial 3 d of AP20187 injections (10 mg/kg) (Fig. 3*A*). After 6 wk, the AP20187 group showed marked reductions of trabecular (55%, Fig. 3*B*) and cortical bone volumes (20%, Fig. 3*C*) via micro computed tomography (μCT) analysis. Furthermore, PTH showed no anabolic effects on either trabecular or cortical bones in the AP20187 group (Fig. 3 *B* and *C*), whereas controls showed significant increases in trabecular (20%, Fig. 3*B*) and cortical bone (7%, Fig. 3*C*) in response to PTH treatment. Histomorphometric analysis showed that PTH-dependent increases in trabecular bone area, thickness, and number and reciprocal decreases of trabecular spaces were attenuated in the AP20187 compared with control group (Fig. 4*A*). These changes were amplified in histomorphometric analysis compared with micro CT analysis, which focused on a narrow region of interest in the metaphyseal area. Osteoclast numbers (OC.N/BS) in tartrate resistant acid phosphate (TRAP)-stained sections (Fig. 4*B*) and serum TRAP5b levels (Fig. 4*C*) were significantly increased with PTH treatment in controls, whereas these PTH effects were lost in the AP20187 group. Furthermore, serum P1NP levels were also increased with PTH in controls, but not in the AP20187 group (Fig. 4*D*), suggesting that PTH induced bone remodeling was attenuated in the macrophage-depleted MAFIA mouse model.

Anabolic Actions of PTH in the Clodronate Liposome Macrophage Depletion Model. The MAFIA mouse model results in a dramatic reduction of all c-fms$^+$ cells. The next approach was focused to deplete mature phagocytic macrophages using clodronate liposomes (22). Intraperitoneal injection of clodronate liposomes (10 μL/g) resulted in 80% depletion of GR1$^-$F4/80$^+$SSC$^{int/lo}$ cells at 24–48 h, with more than 50% of the depleted cells recovered after 72 h (Fig. S5). Hence, clodronate liposomes or PBS liposomes (10 μL/g) were injected for the initial three consecutive days then every third day for 3 wk, and a reduced dose (6 μL/g) was used for the final 3 wk (Fig. 5*A*). After 6 wk of clodronate liposome injections, flow cytometric analyses demonstrated that GR1$^-$F4/80$^+$SSC$^{int/lo}$ macrophages were depleted by 65% (Fig. 5*B*). In notable contrast, CD68$^+$ phagocytic cells were increased

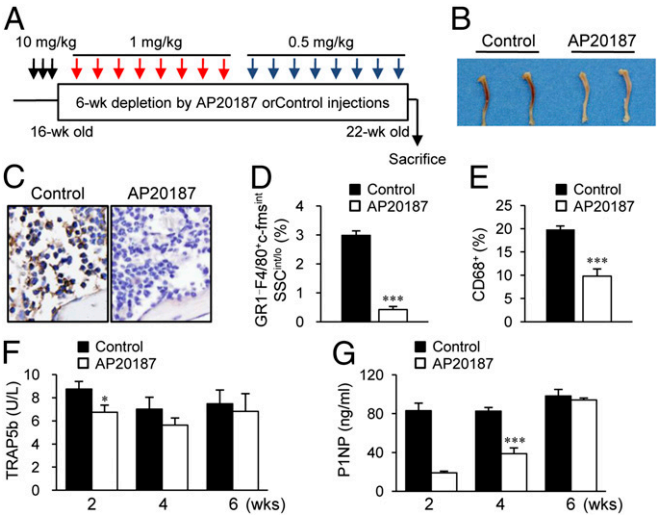

Fig. 2. Long-term depletion of myeloid cells in MAFIA mice. (*A*) Macrophage depletion regimen. MAFIA mice (16 wk old, female) were treated with three consecutive AP20187 (10 mg/kg) injections (black arrows), followed by booster injections every third day (1 mg/kg for 3 wk, then 0.5 mg/kg for 3 wk; red and blue arrows, respectively). (*B*) Photographic representation and (*C*) F4/80$^+$ immunohistochemical staining of tibiae harvested after 6-wk AP20187 or control treatments. Flow cytometric quantification of (*D*) GR1$^-$F4/80$^+$c-fms^{int}SSC$^{int/lo}$ and (*E*) CD68$^+$ cells. Serum samples were collected at 2-, 4-, and 6-wk time points during the 6-wk AP20187 treatment period. (*F*) TRAP5b (units per liter) and (*G*) P1NP (nanograms per milliliter) were measured. Data are mean ± SEM of two independent experiments. $n = 6$–10 per group. $^*P < 0.01$; $^{***}P < 0.001$ versus control.

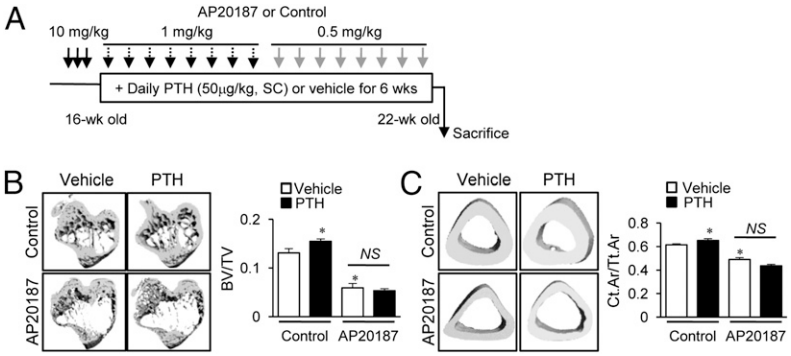

Fig. 3. μCT analyses of bone in long-term depleted MAFIA mice. (*A*) Treatment regimen with PTH and AP20187. MAFIA mice (16 wk old, female) were treated with three consecutive AP20187 (10 mg/kg) injections, followed by booster injections every third day (1 mg/kg for 3 wk, then 0.5 mg/kg for 3 wk). Six weeks of intermittent PTH (50 μg/kg) were started after the initial 3 d. Representative images and quantitative analyses of μCT scanning of tibiae for (*B*) trabecular bone volumes and (*C*) fractional cortical bone areas. All data are means ± SEM of two independent experiments. $n = 8$–10 per group. NS, not significant; $^*P < 0.05$ versus vehicle-treated control.

by 20% (Fig. 5*C*) and $CD11b^+GR1^+F4/80^-$ immature myeloid cells were robustly increased by 60% (Fig. 5*D*).

In contrast to the MAFIA model, long-term depletion of macrophages with clodronate liposomes resulted in high bone mass, independent of PTH (Fig. 5 *E* and *F*). The μCT analyses demonstrated that the trabecular bone volume was significantly increased (20%) in the clodronate versus PBS liposome group (Fig. 5*E*), with no difference noted in cortical bone volume (Fig. 5*F*). Consistently, histomorphometric analysis showed that trabecular bone area and trabecular numbers were significantly increased by 64% and 70%, respectively, and trabecular spacing was reciprocally reduced by 40% in the clodronate versus PBS liposome groups (Fig. 6*A*).

More interestingly, anabolic actions of PTH were even greater in mice administered clodronate versus PBS liposomes. μCT analyses showed PTH-dependent increases of trabecular bone mass were significantly higher in the clodronate versus PBS liposome groups (50% versus 20%, $P < 0.05$, Fig. 5*E*). Furthermore, histomorphometric analyses consistently revealed that PTH enhanced trabecular bone area (96% versus 63%, $P < 0.05$) and trabecular number (57% versus 47%, $P < 0.05$) with clodronate versus PBS liposome treatment (Fig. 6*A*). TRAP staining showed that basal numbers and PTH-dependent increases in osteoclast numbers were similar between the PBS and clodronate liposome groups (Fig. 6*B*).

To further investigate bone remodeling in this model, serum bone turnover markers, including P1NP and TRAP5b, were measured at 4 and 6 wk. As shown in Fig. 6*C*, serum P1NP levels were significantly increased in the clodronate liposome group (30%), and PTH-mediated increases of P1NP were higher in clodronate versus PBS liposome groups with marginal significance (Δ50% versus Δ81%, $P = 0.07$) at 4 wk (Fig. 6*C*). However, basal serum TRAP5b levels and PTH-dependent increases were similar between clodronate and PBS liposome groups at both 4 and 6 wk (Fig. 6*D*). Collectively, clodronate treatment resulted in higher bone mass and amplified PTH anabolism with paralleled increases in serum P1NP, suggesting that these bone changes resulted from enhanced bone formation rather than inhibition of bone resorption.

Clodronate-Targeted Macrophages Stimulated the Mononuclear Phagocytic System. In contrast to the MAFIA mouse model, depletion of macrophages by clodronate liposomes resulted in high bone mass with enhanced PTH anabolic actions. A key difference between the MAFIA and clodronate liposome mouse models was the change in $CD68^+$ cells. Although $GR1^-F4/80^+SSC^{int/lo}$ macrophages were reduced in both MAFIA and clodronate liposome models, the percentages of $CD68^+$ cells were oppositional. $CD68^+$ cells were decreased in the MAFIA mouse model (Fig. 2*E*) and increased in the clodronate mouse model (Fig. 5*C*). Because CD68 has been referred to as an antigen-presenting phagocyte (19, 20), we evaluated the bone marrow microenvironmental changes in the clodronate liposome mouse model.

TUNEL staining of bone sections after 6 wk of treatment revealed that the increase of $TUNEL^+$ apoptotic cells in clodronate liposome-treated mice was much less than that in the MAFIA mouse model (fourfold versus 18-fold, $P < 0.01$, Fig. 7 *A* and *B*). Because both clodronate liposomes and MAFIA/AP20187 injections resulted in similar macrophage depletions at 6 wk, 85% (Fig. 2*D*) and 75% (Fig. 5*B*), respectively, we deduced that cell clearing processes were activated in the clodronate liposome mouse model, which resulted in the notable differences of $TUNEL^+$ cells between MAFIA and clodronate liposome mice. Indeed, flow cytometric analyses showed that cells stained

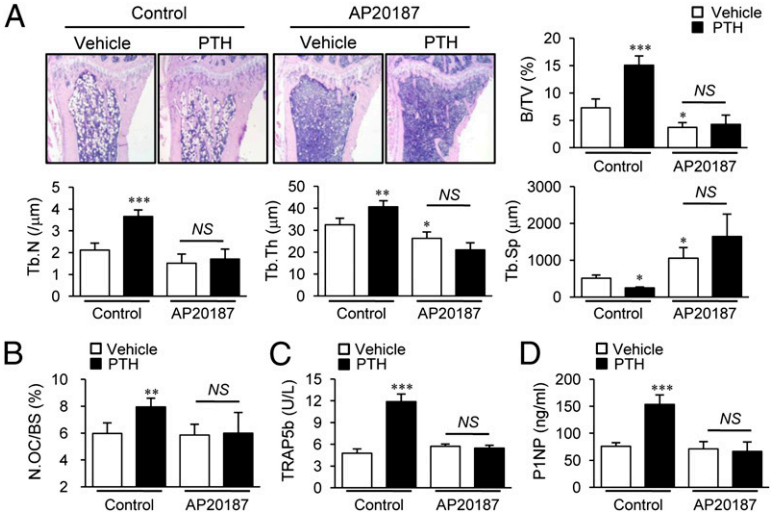

Fig. 4. Bone histomorphometric and serum analyses in long-term depleted MAFIA mice. Histomorphometric analyses of tibiae using the experimental design in Fig. 3*A*. (*A*) Histologic images and static morphometric parameters, including bone volume (BV/TV), trabecular number (Tb.N), trabecular thickness (Tb.Th), and trabecular spacing (Tb.Sp). (*B*) $TRAP^+$ osteoclast numbers (N.OC/BS) were determined. Serum (*C*) TRAP5b (units per liter) and (*D*) P1NP (nanograms per milliliter) levels determined at 6 wk. Data are mean SEM of two independent experiments. $n = 8$–10 per group. NS, not significant; $^*P < 0.05$; $^{**}P < 0.01$; $^{***}P < 0.001$ versus vehicle-treated control (the leftmost column of each graph).

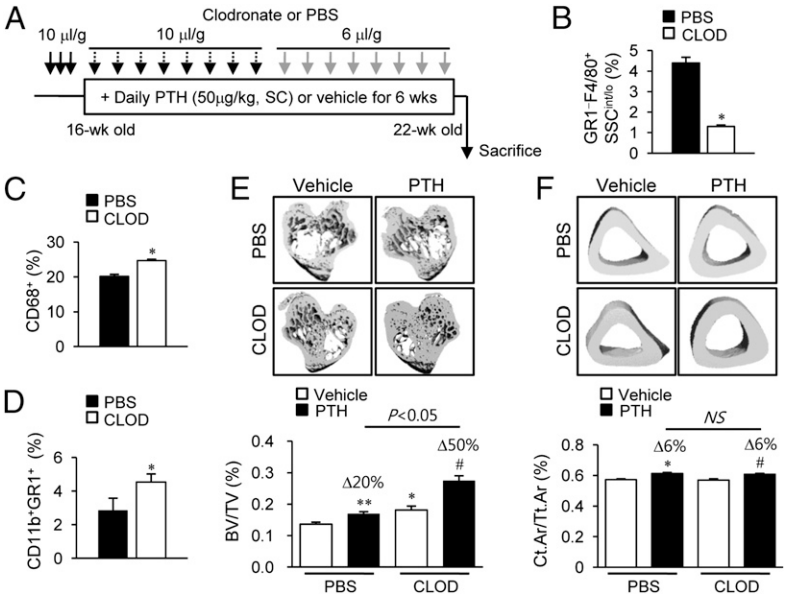

Fig. 5. Bone marrow FACs and μCT analyses in clodronate liposome-treated mice. (*A*) Treatment regimen with clodronate liposomes and PTH. Mice (16 wk old, female) were treated with three consecutive injections of clodronate liposomes (10 μL/g), followed by booster injections every third day (10 μL/g for 3 wk, then 6 μL/g for 3 wk). Six weeks of intermittent PTH (50 μg/kg) were started 3 d after the initiation of clodronate treatment. (*B–D*) Flow cytometric analyses of the whole bone marrow cells. Quantitative analyses of (*B*) $GR1^{-}F4/80^{+}SSC^{int/lo}$ cells, (*C*) $CD68^{+}$ cells, and (*D*) $CD11b^{+}GR1^{+}$ cells. Representative images and graphs (below) of μCT analyses of (*E*) trabecular bone volumes and (*F*) fractional cortical bone areas. Data are mean ± SEM of two independent experiments. n = 10–15 per group. CLOD, clodronate liposome; NS, not significant; PBS, PBS liposome. $^{*}P < 0.05$; $^{**}P < 0.01$ versus vehicle-treated PBS; $^{\#}P < 0.05$ versus vehicle-treated CLOD.

with the $CD163^{+}$ antibody, a member of the scavenger receptor cysteine-rich superfamily (23), were significantly increased with clodronate liposome treatment (Fig. 7*C*).

Bone microenvironments were further investigated. Bone marrow gene expression was investigated after 4 wk of treatment with clodronate liposomes. Real-time PCR analyses showed that genes related to efferocytosis and the M2 phenotype, including *MER receptor kinase*, *milk fat globule-EGF factor 8* (*MFG-E8*), *mannose receptor* (*MRC1*), *macrophage scarvenger receptor 1* (*MSR 1*), *scavenger receptors* (*SR-A* and *CD36*), *IL-10*, and *arginase I*, were up-regulated with clodronate treatment, whereas inflammation-related genes such as *IL-12*, *TNFα*, *IL-1β*, and *iNOS* were not changed between groups (Fig. 7*D*). Protein levels of TGF-β1 were increased with clodronate treatment versus PBS (Fig. 7*E*). Moreover, mRNA expressions of several osteotropic factors known to support PTH anabolic actions were up-regulated in 4-wk-clodronate liposome-treated bone marrow. *TGF-β1* (Fig. 7*F*), *Wnt-3a* (Fig. 7*G*), and *Wnt-10b* (Fig. 7*H*) were up-regulated with clodronate liposome treatment. The PTH-dependent increases in *TGF-β1* (Fig. 7*F*) and *Wnt-3a* (Fig. 7*G*) were higher in clodronate- than in PBS liposome-treated marrows, whereas Wnt-10b was significantly increased by PTH only in the clodronate liposome group (Fig. 7*H*). Collectively, clodronate liposome treatment resulted in increased M2 macrophages as well as increased tissue regenerating factors.

Discussion

The functional role of osteal macrophages was initially established in supporting the maintenance of HSC niches and stimulating intramembranous bone formation in fracture sites (15–17). The actions of macrophages in normal bone remodeling are as yet unclear. The present study showed that osteal macrophages supported bone remodeling in the adult murine skeletal system and that macrophage depletion inhibited PTH anabolic actions in bone. The intriguing finding in this study was that clodronate liposome-induced apoptosis of macrophages paradoxically activated the mononuclear phagocyte system and changed the bone marrow into an osteogenic microenvironment inducing bone formation and augmentation of PTH anabolic actions.

Previous data demonstrated that osteal macrophages stimulated differentiation and mineralization of osteoblasts in vitro,

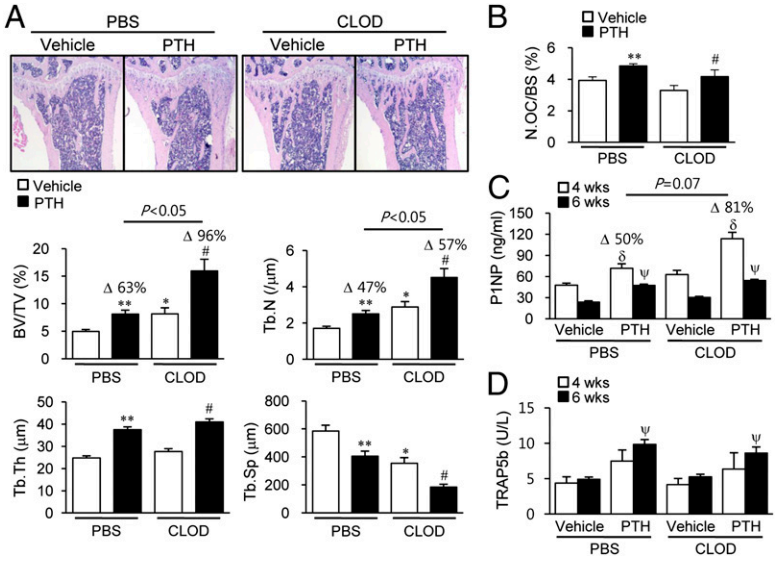

Fig. 6. Bone histomorphometric and serum analyses in clodronate liposome-treated mice. Histomorphometric analyses of tibiae using the experimental design in Fig. 5*A*. (*A*) Representative images with histomorphometric analyses. (*B*) Osteoclast numbers per bone volume (N.OC/BS) measured in TRAP-stained sections. $^{*}P < 0.05$; $^{**}P < 0.01$ versus vehicle-treated PBS. (*C* and *D*) Serum (*C*) P1NP (nanograms per milliliter) and (*D*) TRAP5b (units per liter) measured at 4 and 6 wk. $^{\#}P < 0.05$ versus vehicle-treated CLOD; $^{\delta}P < 0.05$ versus vehicle in each group at 4 wk; $^{\Psi}P < 0.05$ versus vehicle in each group at 6 wk. Data are mean ± SEM of two independent experiments. n = 10–15 per group. CLOD, clodronate liposome; PBS, PBS liposome.

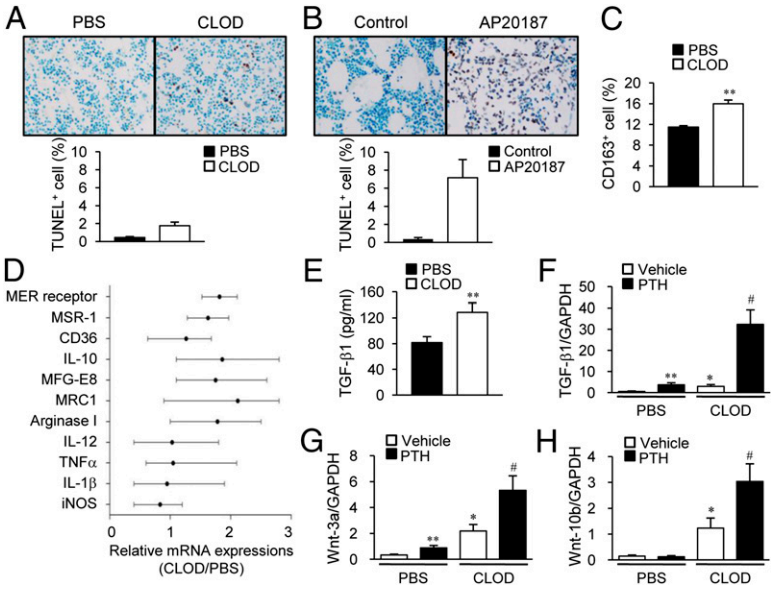

Fig. 7. Bone microenvironment changes in macrophage-depleted mice. (*A*) TUNEL staining on tibial sections in mice (16 wk old, female) treated with clodronate liposomes following the regimen in Fig 5*A*. (*B*) TUNEL staining on tibial sections in mice (16 wk old, female) treated with the regimen in Fig 2*A*. TUNEL$^+$ cells were enumerated. $n = 7$ per group. (*C–E*) Mice (16 wk old, female) were treated with clodronate liposomes; three consecutive injections were followed by booster injections (every third day, 10 μL/g for 3 wk and 6 μL/g for 1 wk). (*C*) Flow cytometric analysis of whole marrow cells using anti-CD163 antibody. (*D*) Genes related to M1/M2 macrophage were analyzed by real-time PCR from whole marrow mRNA. (*E*) Protein levels of TGF-β1 in bone marrow. $^{**}P < 0.01$ versus vehicle. (*F–H*) Mice (16 wk old, female) were treated with clodronate liposomes; three consecutive injections were followed by booster injections (every third day, 10 μL/g for 3 wk and 6 μL/g for 1 wk). Four weeks of intermittent PTH (50 μg/kg) were started after the initial 3 d. Whole marrow mRNA was analyzed by real-time PCR using specific primers for (*F*) *Tgfb1*, (*G*) *Wnt3a*, and (*H*) *Wnt10b*. $^{*}P < 0.05$; $^{**}P < 0.01$ versus vehicle-treated PBS; $^{\#}P < 0.05$ versus vehicle-treated CLOD. Data are mean ± SEM of two independent experiments. $n = 6$ per group. CLOD, clodronate liposome; PBS, PBS liposome.

and depletion of osteal macrophages resulted in loss of mature osteoblasts in bone remodeling sites in vivo (15). The present study further demonstrated that osteal macrophages support bone formation using the MAFIA mouse model. After the 6-wk AP20187 regime, and using the stringent criteria put forth by Chow et al. (21), more than 80% of macrophages were depleted. In contrast, osteoclasts were not significantly affected, likely owing to the staggered administration of the AP20187 after the initial dosing. This suggests that osteoclastogenesis is more robust and/or a preferred pathway of myeloid lineage differentiation in bone.

Both trabecular and cortical bone volumes were significantly decreased with AP20187-induced macrophage depletion. Serum P1NP levels were significantly decreased at 2 (70%) and 4 (50%) wk whereas TRAP5b showed mild suppression in the AP20187-treated group, suggesting that low bone mass in MAFIA depleted mice mainly resulted from the diminution of bone formation. Furthermore, depletion of macrophages with AP20187 treatment completely blocked PTH anabolic actions in bone with inhibition of PTH-dependent increases of the serum bone turnover markers P1NP and TRAP5b. This reinforces the notion that osteal macrophages play a pivotal role in bone anabolism.

To investigate the effects of osteal macrophages on normal bone remodeling and PTH anabolic actions in bone, long-term depletion of macrophages was essential. Because of the critical role of macrophages in general health, it was not feasible to obtain total macrophage depletion without dire consequences. In the present study, several different regimens were tested and the current one was selected with less than 10% mortality and morbidity (infection etc.). Although the depletion percentages of c-fms$^+$ cells were moderate (50%) at 6 wk, further macrophage-specific analyses via flow cytometry, using F4/80 and GR1, showed greater than 80% macrophage depletion via the current regimen and noted alteration in bone phenotypes. The use of the MAFIA mouse in bone biology could seem problematic because osteoclasts might be affected. Indeed, when we used higher or more frequent doses of AP20187 we experienced moderate to severe suppression of osteoclasts with osteopetrotic phenotypes. The mild depletion regimen used in the current study allowed for long-term macrophage-specific reductions to a level that revealed inhibition of bone accrual in normal bone remodeling and PTH anabolic processes.

This study revealed an intriguing finding, that the treatment with clodronate liposomes in vivo paradoxically showed evidence of stimulating the mononuclear phagocyte system for cell clearance, a process termed efferocytosis, and changed the bone microenvironment into one conducive for bone mass accrual and increased PTH anabolic sensitivity. The clodronate liposome model was introduced to further validate the role of osteal macrophages in bone anabolism by using a second and more narrowly focused macrophage depletion model mechanistically unrelated to the MAFIA mouse model. Similar to the MAFIA mouse model, the depletion regimen was adjusted to achieve moderate macrophage depletions with minimum mortality and morbidity. As a result, macrophages reached 65% depletion yet with marked compensatory increases of immature myeloid precursor cells (CD11b$^+$GR1$^+$ cells). One of the notable differences between these two models was that phagocytic myeloid CD68$^+$ cells were reduced in MAFIA mice but increased in clodronate liposome-treated mice. CD68 has been established as a marker for phagocytic myeloid cells including macrophages, dendritic cells, or neutrophils, rather than a specific marker for macrophages (19). These opposite directional changes of CD68$^+$ cell percentages allowed us to hypothesize that selective depletion of macrophages undergoing engulfment with the clodronate liposome treatment led to compensatory increases in myeloid precursor cells and expansion of the activating mononuclear phagocytic system to clear apoptotic cells and debris.

The process of removing dead cell bodies, efferocytosis, is a rapid host defense process for maintaining tissue homeostasis (24). During efferocytosis, apoptotic cells release "find me" and "eat me" signals and are recognized by macrophages or other phagocytic cells. Consistent with CD68$^+$ cells, CD163$^+$ cells (23), another marker for phagocytosis, were also increased in clodronate liposome-treated mice. Furthermore, analysis of gene expression showed that the MFG-E8/MER receptor axis, and the scavenger receptors [CD36 and class A macrophage scavenger receptor (SR-A)] were up-regulated in the clodronate liposome-treated group compared with controls, supporting this hypothesis. This compensatory mechanism was not possible in MAFIA mice, because the AP20187 depletion affected a broad range of c-fms$^+$ myeloid cells, from early precursors to mature macrophages.

More interestingly, M2-macrophage–related genes (IL-10 and arginase I) were increased with reciprocal down-regulation of M1-macrophage–related genes (IL-1, IL-12, iNOS, and TNFα) in the clodronate liposome-treated mice compared with the controls. Macrophages polarize into two different phenotypes (25, 26): M1 macrophages are classically activated by IFNγ or bacterial LPS and have proinflammatory functions, such as regulating antigen presentation to T cells. In contrast, M2 macrophages are alternatively activated by IL-8 or M-CSF and participate in cell clearance or wound healing processes with anti-inflammatory

functions. Recent studies showed that several human pathologic conditions with impaired efferocytosis tend to activate M2 macrophage polarization in an attempt to overcome those pathologic conditions (27–29). This study showed that long-term stimulation of macrophage apoptosis and partial depletion of mature macrophages resulted in not only activation of efferocytosis but also in stimulation of macrophage polarization. In addition, these microenvironmental changes were accompanied by an increase of several osteogenic factors such as canonical Wnts and TGF-β1. Wnt-3a and Wnt-10b represent canonical Wnt family members with well-established strong anabolic signaling in bone. Interestingly, recent studies demonstrated that macrophage-derived Wnt proteins are essential for tissue regeneration in kidney (30, 31) and liver (32). In particular, phagocytosis of apoptotic debris was found to stimulate macrophage production of Wnt-3a, which mediated hepatocyte regeneration (32). Corroborating these previous studies, activated phagocytosis in the present study up-regulated Wnt-3a and Wnt-10b in the bone microenvironment, which provided favorable conditions for bone formation, suggesting that the biologic process of cell clearance is commonly followed by signaling for tissue regeneration.

TGF-β1 is a crucial factor produced during efferocytosis (33, 34) and alternative macrophage polarization (35). It is also released and activated by bone-resorbing osteoclasts and recruits mesenchymal progenitor cells to bone remodeling sites, supporting bone formation (36). In an irradiation-induced bone marrow ablation model, PTH was found to increase bone more robustly in association with increased macrophages and TGF-β1 (13). The up-regulation of TGF-β1 in the present study also links to enhanced bone formation ability and PTH anabolic actions.

Maintaining bone homeostasis is an elaborate process based on cellular interactions between osteoclasts, osteocytes, and osteoblasts, and the coupling of bone resorption to bone formation. The present study demonstrated that osteal macrophages play a role in bone remodeling as another cellular component via supporting bone formation and mediating PTH-dependent anabolic actions in bone. Furthermore, induced efferocytosis, linked to M2 macrophage polarization, transformed the bone microenvironment into an osteogenic one via up-regulating canonical Wnts and TGF-β1 production in bone. In conclusion, osteal macrophages in the bone marrow microenvironment highly and favorably affect bone metabolism in support of regeneration and formation.

Materials and Methods

Two murine models of macrophage depletion included the genetic MAFIA model and a clodronate liposome administered model. After 6 wk of intermittent PTH treatment, bone phenotypes were analyzed histomorphometrically, and via microCT analysis. The bone marrow microenvironment was characterized by standard flow cytometric analyses, immunohistochemical staining, real-time PCR, and biochemical assays. More details are included in *SI Materials and Methods*.

ACKNOWLEDGMENTS. This work was supported in part by the National Institutes of Health Grants DK053904 and CA093900 (to L.K.M.), Department of Defense Grant W81XWH-12-1-0348 (to S.I.P.), and National Medical Center, Research Institute (Seoul, Korea) Grant NMC2013-MS-02 (to S.W.C.).

1. Wu JY, et al. (2008) Osteoblastic regulation of B lymphopoiesis is mediated by Gsalpha-dependent signaling pathways. *Proc Natl Acad Sci USA* 105(44):16976–16981.
2. Calvi LM, et al. (2003) Osteoblastic cells regulate the haematopoietic stem cell niche. *Nature* 425(6960):841–846.
3. Weber JM, et al. (2006) Parathyroid hormone stimulates expression of the Notch ligand Jagged1 in osteoblastic cells. *Bone* 39(3):485–493.
4. Cho SW, et al. (2013) The soluble interleukin-6 receptor is a mediator of hematopoietic and skeletal actions of parathyroid hormone. *J Biol Chem* 288(10):6814–6825.
5. Zhu J, et al. (2007) Osteoblasts support B-lymphocyte commitment and differentiation from hematopoietic stem cells. *Blood* 109(9):3706–3712.
6. Terauchi M, et al. (2009) T lymphocytes amplify the anabolic activity of parathyroid hormone through Wnt10b signaling. *Cell Metab* 10(3):229–240.
7. Li X, Qin L, Partridge NC (2008) *In vivo* parathyroid hormone treatments and RNA isolation and analysis. *Methods Mol Biol* 455:79–87.
8. Onyia JE, Bidwell J, Herring J, Hulman J, Hock JM (1995) *In vivo*, human parathyroid hormone fragment (hPTH 1-34) transiently stimulates immediate early response gene expression, but not proliferation, in trabecular bone cells of young rats. *Bone* 17(5): 479–484.
9. Jung Y, et al. (2006) Regulation of SDF-1 (CXCL12) production by osteoblasts; a possible mechanism for stem cell homing. *Bone* 38(4):497–508.
10. Li X, et al. (2007) Determination of dual effects of parathyroid hormone on skeletal gene expression *in vivo* by microarray and network analysis. *J Biol Chem* 282(45):33086–33097.
11. Li X, et al. (2007) Parathyroid hormone stimulates osteoblastic expression of MCP-1 to recruit and increase the fusion of pre/osteoclasts. *J Biol Chem* 282(45):33098–33106.
12. Adams GB, et al. (2007) Therapeutic targeting of a stem cell niche. *Nat Biotechnol* 25(2):238–243.
13. Koh AJ, et al. (2011) An irradiation-altered bone marrow microenvironment impacts anabolic actions of PTH. *Endocrinology* 152(12):4525–4536.
14. Pirih FQ, et al. (2010) Parathyroid hormone mediates hematopoietic cell expansion through interleukin-6. *PLoS ONE* 5(10):e13657.
15. Chang MK, et al. (2008) Osteal tissue macrophages are intercalated throughout human and mouse bone lining tissues and regulate osteoblast function *in vitro* and *in vivo*. *J Immunol* 181(2):1232–1244.
16. Alexander KA, et al. (2011) Osteal macrophages promote *in vivo* intramembranous bone healing in a mouse tibial injury model. *J Bone Miner Res* 26(7):1517–1532.
17. Winkler IG, et al. (2010) Bone marrow macrophages maintain hematopoietic stem cell (HSC) niches and their depletion mobilizes HSCs. *Blood* 116(23):4815–4828.
18. Burnett SH, et al. (2004) Conditional macrophage ablation in transgenic mice expressing a Fas-based suicide gene. *J Leukoc Biol* 75(4):612–623.
19. Kunisch E, et al. (2004) Macrophage specificity of three anti-CD68 monoclonal antibodies (KP1, EBM11, and PGM1) widely used for immunohistochemistry and flow cytometry. *Ann Rheum Dis* 63(7):774–784.
20. Andreeva ER, Pugach IM, Orekhov AN (1997) Subendothelial smooth muscle cells of human aorta express macrophage antigen in situ and *in vitro*. *Atherosclerosis* 135(1): 19–27.
21. Chow A, et al. (2011) Bone marrow CD169+ macrophages promote the retention of hematopoietic stem and progenitor cells in the mesenchymal stem cell niche. *J Exp Med* 208(2):261–271.
22. Van Rooijen N, Sanders A (1994) Liposome mediated depletion of macrophages: mechanism of action, preparation of liposomes and applications. *J Immunol Methods* 174(1-2):83–93.
23. Lau SK, Chu PG, Weiss LM (2004) CD163: A specific marker of macrophages in paraffin-embedded tissue samples. *Am J Clin Pathol* 122(5):794–801.
24. Bratton DL, Henson PM (2011) Neutrophil clearance: When the party is over, clean-up begins. *Trends Immunol* 32(8):350–357.
25. Lawrence T, Natoli G (2011) Transcriptional regulation of macrophage polarization: Enabling diversity with identity. *Nat Rev Immunol* 11(11):750–761.
26. Mantovani A, Sozzani S, Locati M, Allavena P, Sica A (2002) Macrophage polarization: Tumor-associated macrophages as a paradigm for polarized M2 mononuclear phagocytes. *Trends Immunol* 23(11):549–555.
27. Hodge S, et al. (2011) Cigarette smoke-induced changes to alveolar macrophage phenotype and function are improved by treatment with procysteine. *Am J Respir Cell Mol Biol* 44(5):673–681.
28. Mares CA, et al. (2011) Defect in efferocytosis leads to alternative activation of macrophages in Francisella infections. *Immunol Cell Biol* 89(2):167–172.
29. Yamamoto S, et al. (2011) Macrophage polarization by angiotensin II-type 1 receptor aggravates renal injury-acceleration of atherosclerosis. *Arterioscler Thromb Vasc Biol* 31(12):2856–2864.
30. Lin SL, et al. (2010) Macrophage Wnt7b is critical for kidney repair and regeneration. *Proc Natl Acad Sci USA* 107(9):4194–4199.
31. Reddy SM, et al. (2002) Phagocytosis of apoptotic cells by macrophages induces novel signaling events leading to cytokine-independent survival and inhibition of proliferation: Activation of Akt and inhibition of extracellular signal-regulated kinases 1 and 2. *J Immunol* 169(2):702–713.
32. Boulter L, et al. (2012) Macrophage-derived Wnt opposes Notch signaling to specify hepatic progenitor cell fate in chronic liver disease. *Nat Med* 18(4):572–579.
33. Zarin AA, Behmanesh M, Tavallaei M, Shohrati M, Ghanei M (2010) Overexpression of transforming growth factor (TGF)-beta1 and TGF-beta3 genes in lung of toxic-inhaled patients. *Exp Lung Res* 36(5):284–291.
34. Medeiros AI, Serezani CH, Lee SP, Peters-Golden M (2009) Efferocytosis impairs pulmonary macrophage and lung antibacterial function via PGE2/EP2 signaling. *J Exp Med* 206(1):61–68.
35. Gong D, et al. (2012) TGFβ signaling plays a critical role in promoting alternative macrophage activation. *BMC Immunol* 13:31.
36. Tang Y, et al. (2009) TGF-beta1-induced migration of bone mesenchymal stem cells couples bone resorption with formation. *Nat Med* 15(7):757–765.